DOT/FAA/TC-18/14

Modeling of Hidden Fire in Aircraft Overhead Area

February 2019

Final Report

This document is available to the U.S. public through the National Technical Information Services (NTIS), Springfield, Virginia 22161.

This document is also available from the Federal Aviation Administration William J. Hughes Technical Center at actlibrary.tc.faa.gov.

U.S. Department of Transportation
Federal Aviation Administration

NOTICE

This document is disseminated under the sponsorship of the U.S. Department of Transportation in the interest of information exchange. The U.S. Government assumes no liability for the contents or use thereof. The U.S. Government does not endorse products or manufacturers. Trade or manufacturers' names appear herein solely because they are considered essential to the objective of this report. The findings and conclusions in this report are those of the author(s) and do not necessarily represent the views of the funding agency. This document does not constitute FAA policy. Consult the FAA sponsoring organization listed on the Technical Documentation page as to its use.

This report is available at the Federal Aviation Administration William J. Hughes Technical Center's Full-Text Technical Reports page: actlibrary.tc.faa.gov in Adobe Acrobat portable document format (PDF).

1. Report No.	2. Government Accession No.	3. Recipient's Catalog No.
DOT/FAA/TC-18/14		

4. Title and Subtitle	5. Report Date
MODELING OF HIDDEN FIRE IN AIRCRAFT OVERHEAD AREA	February 2019
	6. Performing Organization Code
	ANG-E2

7. Author(s)	8. Performing Organization Report No.
Haiqing Guo[1], Ezgi S. Oztekin[2], Sean Crowley[3], Paul Scrofani[4], Richard E. Lyon[3]	

9. Performing Organization Name and Address	10. Work Unit No. (TRAIS)
[1] CFar Services, 303 Quail Dr., Marmora, NJ 08223 [2] Diakon Solutions, 110 W Beaver Dr., Cape May Court House, NJ 08210 [3] Federal Aviation Administration, William J. Hughes Technical Center, Atlantic City Airport, NJ 08405 [4] Galaxy Scientific Corporation, 2628 Fire Rd., Egg Harbor Township, NJ 08234	
	11. Contract or Grant No.

12. Sponsoring Agency Name and Address	13. Type of Report and Period Covered
U.S. Department of Transportation FAA Northwest Mountain Regional Office 1601 Lind Avenue SW Renton, WA 98057	Final Report
	14. Sponsoring Agency Code
	AIR-600

15. Supplementary Notes
The FAA William J. Hughes Technical Center Aviation Research Division COR was Robert Ochs.

16. Abstract

Hidden fire in the aircraft cabin has been characterized as a hazardous phenomenon to in-flight safety and could lead to catastrophic disaster. Detecting hidden fire at the earliest stage is required and can be achieved only through an improved understanding of the transport of hot gases and smoke due to a possible hidden fire. This research uses the computation fluid dynamics tool to simulate the heat and mass transport in situations of hidden fire in the overhead area of the aircraft cabin. The modeled temperatures are compared with the full-scale test results, and reasonable agreements are observed. The simulation also presents comprehensive hot gas transport information. Further investigations are performed to examine the effect of ambient pressure and the fire source location. It is found that at cruise altitude with reduced ambient pressure, ceiling temperature increases as a result of increased flame height and decreased air entrainment. The ceiling temperature is sensitive to the fire source location. Hot gases tend to migrate to the highest ceiling location. Obstruction thicker than the ceiling jet boundary layer at the ceiling level can result in extra hot spots.

17. Key Words	18. Distribution Statement
Hidden fire, Aircraft overhead, Computational Fluid Dynamics, Ceiling jet	This document is available to the U.S. public through the National Technical Information Service (NTIS), Springfield, Virginia 22161. This document is also available from the Federal Aviation Administration William J. Hughes Technical Center at actlibrary.tc.faa.gov.

19. Security Classif. (of this report)	20. Security Classif. (of this page)	21. No. of Pages	22. Price
Unclassified	Unclassified	35	

Form DOT F 1700.7 (8-72)   Reproduction of completed page authorized

TABLE OF CONTENTS

LIST OF FIGURES

LIST OF ACRONYMS

AC	Advisory Circular
CAD	Computer-aided design
CFD	Computational Fluid Dynamics
FDS	Fire Dynamics Simulator
LIDAR	Light detection and ranging

EXECUTIVE SUMMARY

This study researches the heat and mass transport as a result of a fire source in the hidden area located in the overhead space of the aircraft test article cabin. The overhead area involves complex geometry, a highly curved ceiling, and densely cluttered obstructions. It presents a challenge to aircraft fire safety and, more specifically, to timely fire detection and suppression. Visual observation of major fire signatures, such as flame luminance and smoke, in the hidden area is usually delayed and less reliable. Therefore, fire in the hidden area must be detected at the earliest stage, which further requires better understanding of the heat and mass (including hot gases and smoke) transport within complex geometry.

The current research focuses only on the hot gas transport by measuring the temperature rise at the ceiling level as a result of a fire source. Smoke is not introduced in the fire source because of the potential contamination to the test article. It is speculated that smoke carried by the buoyancy plume will follow the hot gas movement in the overhead area. Qualitative assessment of the smoke density is not within the scope of the current study.

In addition to the full-scale fire test in the aircraft overhead area, Computational Fluid Dynamics (CFD) is used as a primary tool in this study. CFD carries the advantages of lower cost, faster assessment of design variations, more comprehensive information, and ability to explore conditions not possible in full-scale tests. The CFD simulations were performed using the high-performance computing system built at the FAA William J. Hughes Technical Center at the Atlantic City International Airport, NJ. This system has more than 200 computation cores and can significantly reduce computation time through parallel computation.

The following tasks were accomplished during this research:

Task 1:   Performed full-scale fire tests at the selected region in the test article Boeing 747-SP cabin overhead area. The test measures the ceiling temperature at 50 thermocouple locations at the ceiling level and allows the vertical temperature gradient to be assessed using thermocouples at different heights.

Task 2:   Imported the computer-aided design model of the overhead area to the CFD model, and generated a mesh system for the imported geometry. Each mesh is assigned to one computation core.

Task 3:   Performed CFD simulation at the full-scale test condition. The simulated results are compared with the test results for validation.

Task 4:   Performed CFD simulation at reduced pressure. The simulated results are compared with the simulation at normal pressure for pressure effect.

Task 5:   Performed CFD simulation with different fire source locations.

CFD is found to predict the temperature field very well. CFD also revealed that the lower ambient pressure at cruise altitude decreases air entrainment in the fire and, therefore, results in a higher ceiling temperature. Complex geometries at the ceiling height obstruct the gas flow and create hot spots.

A comprehensive study (both experiments and simulations) of the transport of heat, smoke, and carbon monoxide/dioxide from burning solid fuels in the cluttered spaces (e.g., cargo compartment, cabin, overhead area) is anticipated in the future. Besides the pressure's effect on fire size, air entrainment, and plume movement, and its effect on solid fuel pyrolysis rate, combustion products (especially smoke) are to be studied. The results from the current study combined with those studies will be used to guide the placement and certification of smoke detectors, temperature sensors, and CO detectors in transport and cargo aircraft.

1. INTRODUCTION

The FAA Advisory Circular (AC) 120-80A [1] defines hidden fires as those that are not readily accessible, may be difficult to locate, and that are more challenging to extinguish. Figure 1 shows the diagram of a typical wide-body aircraft cross-section with possible locations of hidden fires [1]. Causes of in-flight fires include wiring failures, electrical component failures, lightning strikes, and overheating of batteries. The indications of hidden fires include abnormal operation or disassociated component failures, circuit breakers, hot spots, fumes, and visual sighting of smoke. In particular, the plume induced by the fire source, coupled with the generated smoke, are the signatures of a hidden fire at the earliest stage.
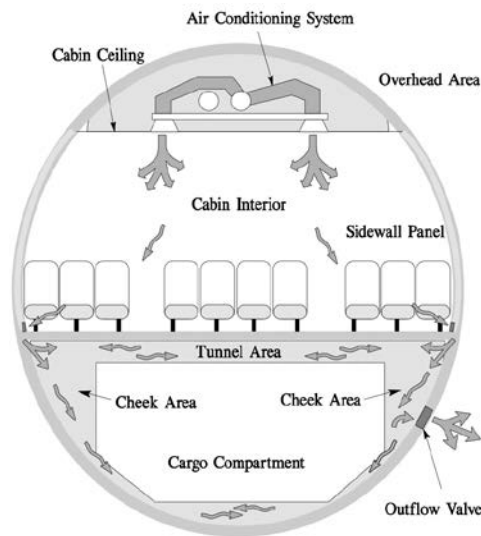
Figure 1. Airplane cross-section showing possible locations of hidden-area fires

Hidden fires always involve solid material pyrolysis and combustion, and the heat output from burning is complex and unsteady. Zhang et al. [2] showed that a gas burner can be used to emulate the steady burning of condensed phase fuel by matching the smoke point, heat of combustion, and flame height. It has the advantage of better controllability- the burner can be instantaneously shut off in the event of an emergency during the full-scale test.

Unlike the traditional open compartment fire, the hidden area in the aircraft involves more complex geometry, more obstruction along the plume path and highly curved ceiling surface. Performing full-scale fire tests in the test article is expensive, sometimes destructive, and, more importantly, highly hazardous. The number of fire scenarios to be tested increases significantly when considering the variance in potential fire source, fire location, and cabin configuration. In addition, the in-flight fire at the cruise altitude always involves reduced cabin pressure, which cannot be practically achieved in ground-based testing. There are some large pressure chambers, but to do a fire test in them would be very costly.

1

These considerations warrant the use of a Computational Fluid Dynamics (CFD) tool to study the plume movement in the aircraft hidden area. CFD has the advantages of lower development cost, faster assessment of design variations, more comprehensive information, and the ability to explore conditions that are difficult or impossible to achieve in ground-based, full-scale testing.

The objectives of the present study are to choose one representative fire scenario in the cabin overhead area, perform a full-scale fire test, and run numerical simulations of the chosen scenario. The simulated results will be compared to the test results for validation purposes. Numerical simulations of the scenario with reduced pressure will be examined to understand the pressure effect on plume movement. Numerical simulations of the scenario with different burner locations will also be examined to reveal the burner location effect.

2. METHODOLOGY

2.1 EXPERIMENTAL

The focus of the present study is the hidden fires that may occur in the overhead area of an aircraft cabin. Figure 2 shows the test article Boeing 747-SP located at the FAA William J. Hughes Technical Center. Only a selected region, shown in red in the figure, was studied. The dimensions of this region are 6.7 m long × 5.4 m wide × 2 m tall. The cross-section of the overhead space changes with the contour of the exterior skin, with ribs located every half meter. The contents of the overhead space include air-distribution ducts, flight-control cables, electrical wiring, and support structures.

Figure 2. Test article Boeing 747-SP; area of interest is shown in red

Light detection and ranging (LIDAR) technology was used to generate the 3-D CAD model of the overhead area. An overview of the LIDAR-generated 3-D CAD model of the overhead area is shown in figure 3.
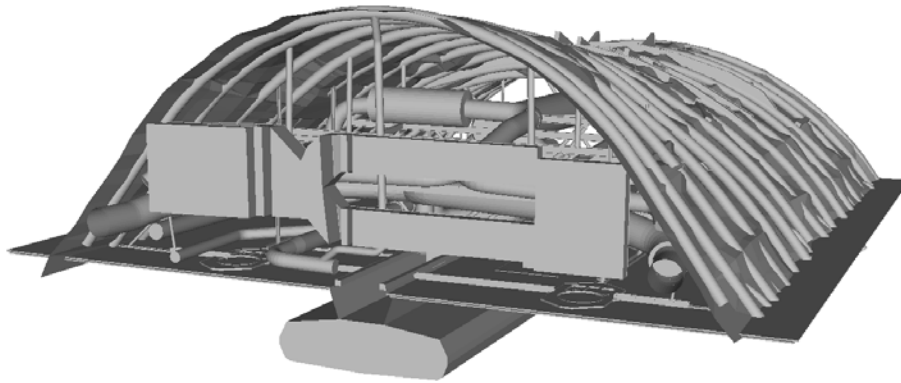
Figure 3. Overview of the LIDAR generated 3-D CAD model of the test article Boeing 747 cabin overhead area

A gas burner fueled with propane was used as a fire source in the full-scale test. The gas burner is rectangular with 178 mm sides and 210 mm depth. A mass flow controller (Alicat: MC-20SLPM) was used to adjust the fuel-flow rate. In the present test and simulation, a constant propane flow rate is used to generate a steady heat release rate of 11 kW.

To map out the hot gas movement and temperature distribution at the ceiling level, the overhead area was equipped with 50 thermocouples (Type K, 36-AWG). The thermocouples were laid on the ribs and placed 5 cm below the insulated ceiling. Figure 4 is an aerial view of the thermocouples on the curved ceiling. The first row of thermocouples is 0.46 m from the front panel. Thermocouples 49/50 and 41/42 are 0.67 m from the edges. Figure 4 also shows the thermocouple tree (A and B) location on each side of the propane burner location (marked as a red X). Each thermocouple tree has four thermocouples, with the top one 5 cm below the ceiling and a 15 cm separation distance between thermocouples. The center of the propane gas burner is 1.25 m away from the front panel and 2 m from the near edge.
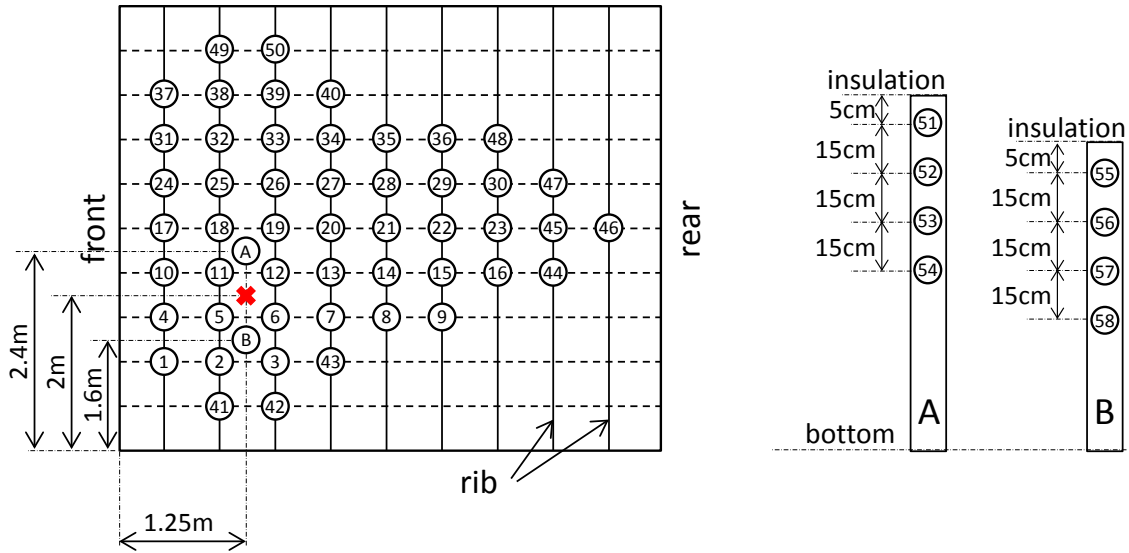
Figure 4. Detailed layout of the thermocouple and thermocouple tree

2.2 NUMERICAL

The fire simulation was performed using the Fire Dynamics Simulator (FDS), developed by the National Institute of Standards and Technology. FDS is a large-eddy simulation code for low-speed, thermally/buoyancy driven flows, developed to simulate smoke and heat transport from fires.

This research is focused on the Boeing 747-SP test article overhead area. The total computation domain is the overhead space in a curved fuselage section 6.7 m × 5.4 m × 2 m. The narrow structures (tubing, wires, etc.) were excluded from the model for simplicity. The structures at the bottom of the overhead area are also excluded because they are far away from the plume and have negligible effect on the plume temperature. The simplified model in the FDS simulation is shown in figure 5. The burner is marked in red. Figure 6 shows the front, side, and top views of the overhead area. The insulation layer is hidden.
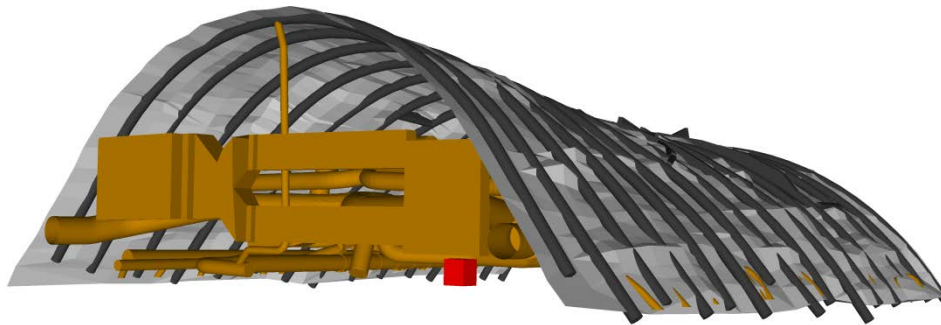
Figure 5. Simplified CAD model of the test article Boeing-747 cabin overhead area used in FDS simulation
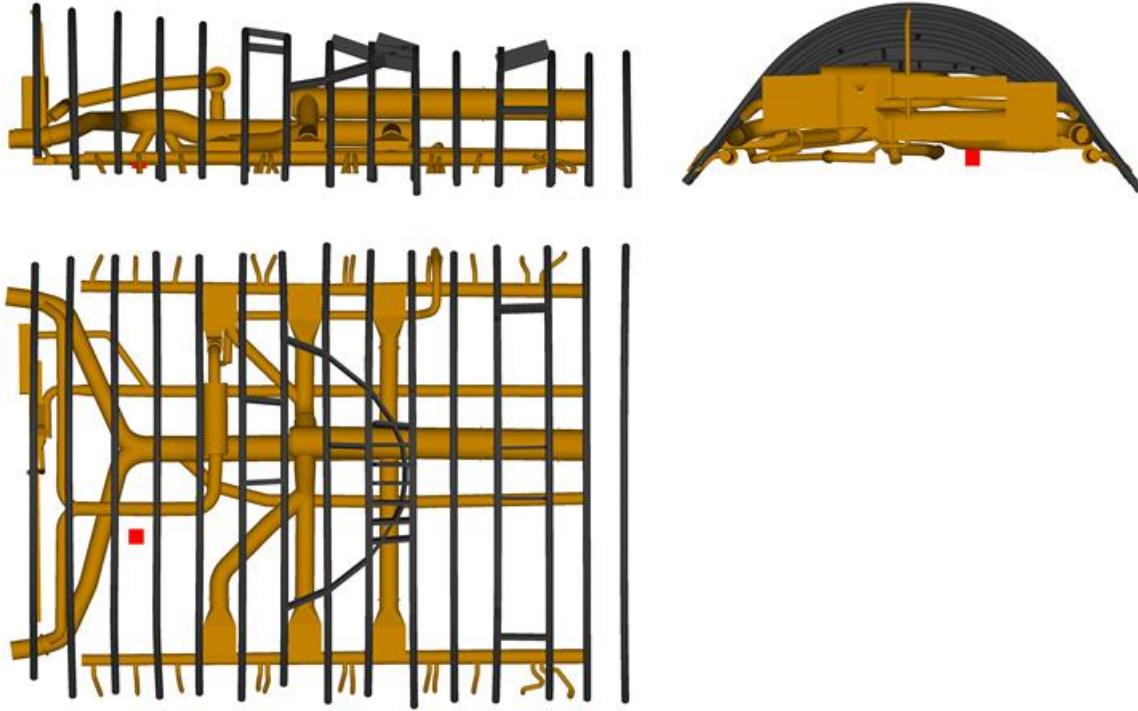
Figure 6. The front view, side view and top view of the test article Boeing-747 cabin overhead area

The overhead area computational domain was evenly divided into 84 meshes, each of which is handled by one computational core in the FAA's high-performance computing system. The mesh size is uniformly 2 cm, except for the critical regions (i.e., the gas burner and its adjacent locations), which have a mesh size of 1 cm. The characteristic fire size, D^*, defined as:

$$D^* = \left[\frac{\dot{Q}}{\rho_\infty c_p T_\infty \sqrt{g}} \right]^{2/5}, \tag{1}$$

D* is 0.16 m for a typical fire with a heat release rate of 11 kW. The resulting nondimensional expression $D^* / \delta x = 0.16\text{m}/0.01\text{m} = 16$, which satisfies the general requirement that the nondimensional fire size needs to be at least 10 to adequately resolve the flow field involving buoyant plumes [3].

The model assumes simple chemistry reaction in the form:

$$C_3 H_8 + 5(O_2 + 3.73 N_2) = 3CO_2 + 4H_2 O + 18.65 N_2 \tag{2}$$
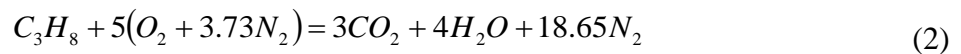
In the well-ventilated condition, incomplete combustion products of CO and soot are neglected. The propane heat of combustion ΔH_c is 46.4 kJ/g. The total heat release rate from the burner surface is 11 kW. The radiative fraction is taken to be 0.3.

5

Preliminary simulations assumed an adiabatic surface at the ceiling insulations. The simulated temperature results were expected to be higher than the test results because no conductive heat loss through the ceiling was considered. Alternatively, the properties of the real insulation material were used. The insulation incudes a layer of fiberglass (thermal conductivity $k = 0.04$ W/m-K) followed by a layer of ceramic paper ($k = 0.05$ W/m-K). The additional ceramic paper is added to prevent the insulation layer from burning during the fire test. Conductivity of the metal airplane body behind this insulation is considered to be negligible. A single, equivalent thermal conductivity was used to represent the combined effect of fiberglass and ceramic paper.

In the full-scale test, the front panel was covered with plastic membrane. It was simplified as an isothermal surface in FDS. The bottom panel was also modeled as an isothermal surface. The rear side is modeled open to ambient condition. The ambient condition is set at 20°C and 1 bar.

During the ground level simulation, the cabin overhead area pressure was 1 bar. However, due to concerns about the effect of in-flight pressure on flame height, plume spread, and temperature distribution at the ceiling level, an extra simulation was performed with the exact same setup, but with lower ambient pressure, at 0.75 bar. This corresponds to atmospheric pressure at 2438 m (8000 feet) above sea level. The effect of low (in flight) pressure on the burning of solid fuel and smoke yield has been reported [4, 5] but was not included in the present simulations. In the present study, a gas burner with a steady fuel supply is used, and propane does not generate soot at the experimental flow rate. Therefore, the effect of ambient pressure on burning of aircraft materials was not addressed in the present study.

In simulations, the gas burner is also shifted along the x-axis toward the rear end of the overhead area and computational domain to examine the burner location effect. The distance between the burner center and the computational domain end is 1.25 m. At this location, the ceiling height is approximately 0.5 m lower than in the original forward location. Hot gases are expected to rise, following the contour of the ceiling towards the higher forward end in the front of the overhead area. Full-scale test validation has not yet been performed for this scenario. The gas temperature sensor locations were kept the same.

3. RESULTS

Both tests and simulations were conducted for 300 s durations. In tests, temperatures within 60 s before ignition were averaged and used as a baseline. The temperatures were then manually shifted to have baselines at 20°C, to be consistent with the simulation setting. The tests were repeated three times and the temperatures agreed within 5 C between replicas. The averaged values were used. The results were presented in the following manner: 1) the simulated results were compared with the test results at normal pressure ($p = 1$ bar); 2) the simulated results at reduced pressure ($p = 0.75$ bar) were compared with the simulated results at normal pressure to examine the pressure effect; 3) at normal pressure, the simulated results with different burner locations were discussed.
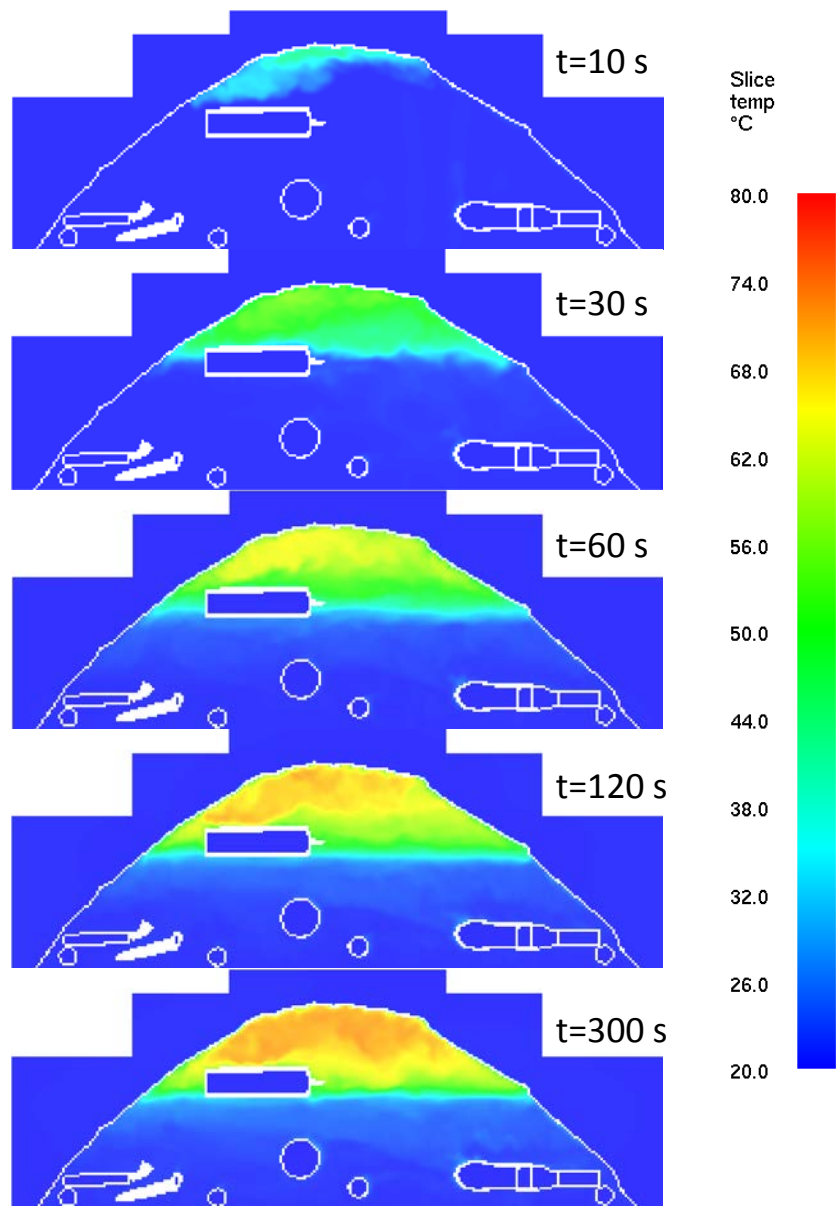
3.1 NORMAL PRESSURE RESULTS

Figures 7 and 8 show the simulated temperature slices from a normal pressure scenario, on the y-z plane, at $x = 2.25$ and 3.25 m, respectively. Time was selected at $t = 10, 30, 60, 120,$ and 300 s for the effect of plume and ceiling jet development. Figures 9 and 10 show the simulated
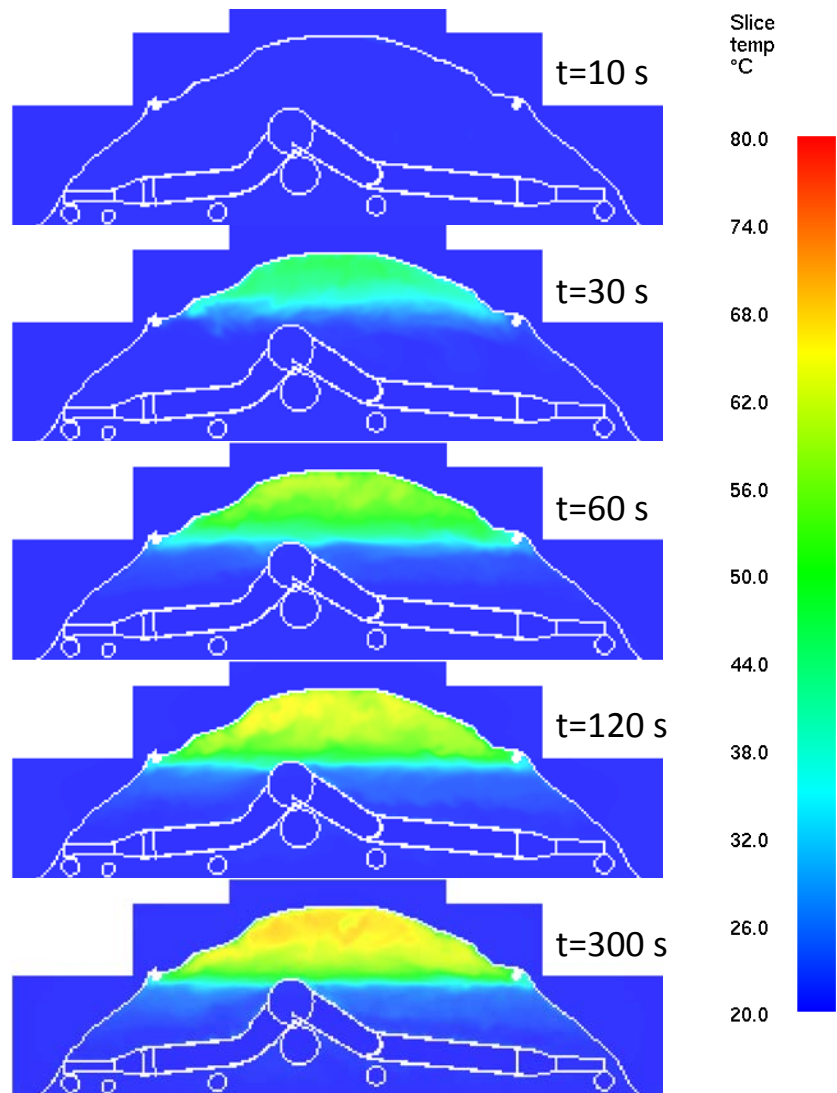
temperature slices on the x-z plane, at $y = 3$ and 3.5 m, respectively. Hot gases are seen rising and spreading toward the edges and the tail simultaneously. The ceiling jet layer accumulates; with the layer temperature constantly increasing, until it reaches the steady state. The maximum temperature on the slices is approximately 80°C.

An obvious time delay can be observed along the y-axis because the hot gas spreads a longer distance (approximately 5 m), as indicated in figures 9 and 10. In addition, because the center in the front region is higher than that in the rear region, hot gases tend to fill the higher space before spreading to the lower region at the rear end. The hot gas layer (approximately 0.5 m thick at $x = 2.25$ m) develops very quickly within the initial 30 s. The ceiling jet layer is much thicker than the rib thickness of approximately 0.1 m. Therefore, the rib has a negligible effect in hindering the gas-flow movement. Conversely, the panels under ribs 9, 10, and 12 are big enough to provide sufficient obstruction to the gas flow. Large swirls can be observed near these regions in figures 9 and 10.

Similarly, figures 11 and 12 show the simulated velocity results on the y-z plane, at $x = 1.25$ m, and on the x-z plane, at $y = 2$ m. Time was selected at $t = 10$, 60, and 300 s. These two planes cross the burner center. Figure 11 shows that after the plume hits the ceiling, it moves toward the center, which has a higher elevation. Air movement in the compartment increases with the ceiling temperature because of the increased convection between the hot gas layer and the cold zone beneath it. The maximum jet velocity was found to be approximately 1.5 m/s.
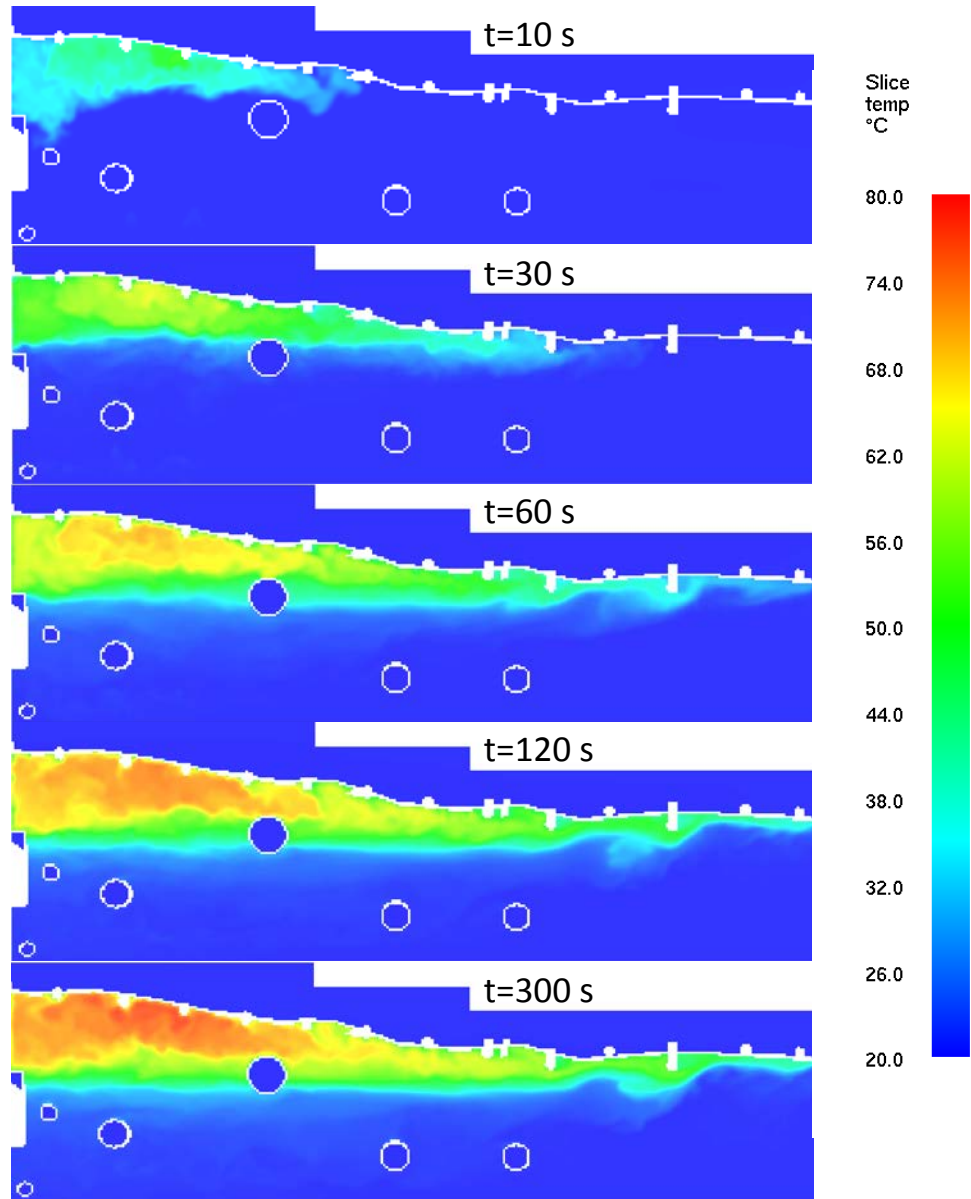
Figure 7. Simulated temperature slice results from normal pressure scenario ($p = 1$ bar) on the y-z plane at $x = 2.25$ m; time was selected at $t = 10, 30, 60, 120,$ and 300 s

Figure 8. Simulated temperature slice results from normal pressure scenario ($p = 1$ bar) on the *y-z* plane at *x* = 3.25 m; time was selected at *t* = 10, 30, 60, 120, and 300 s
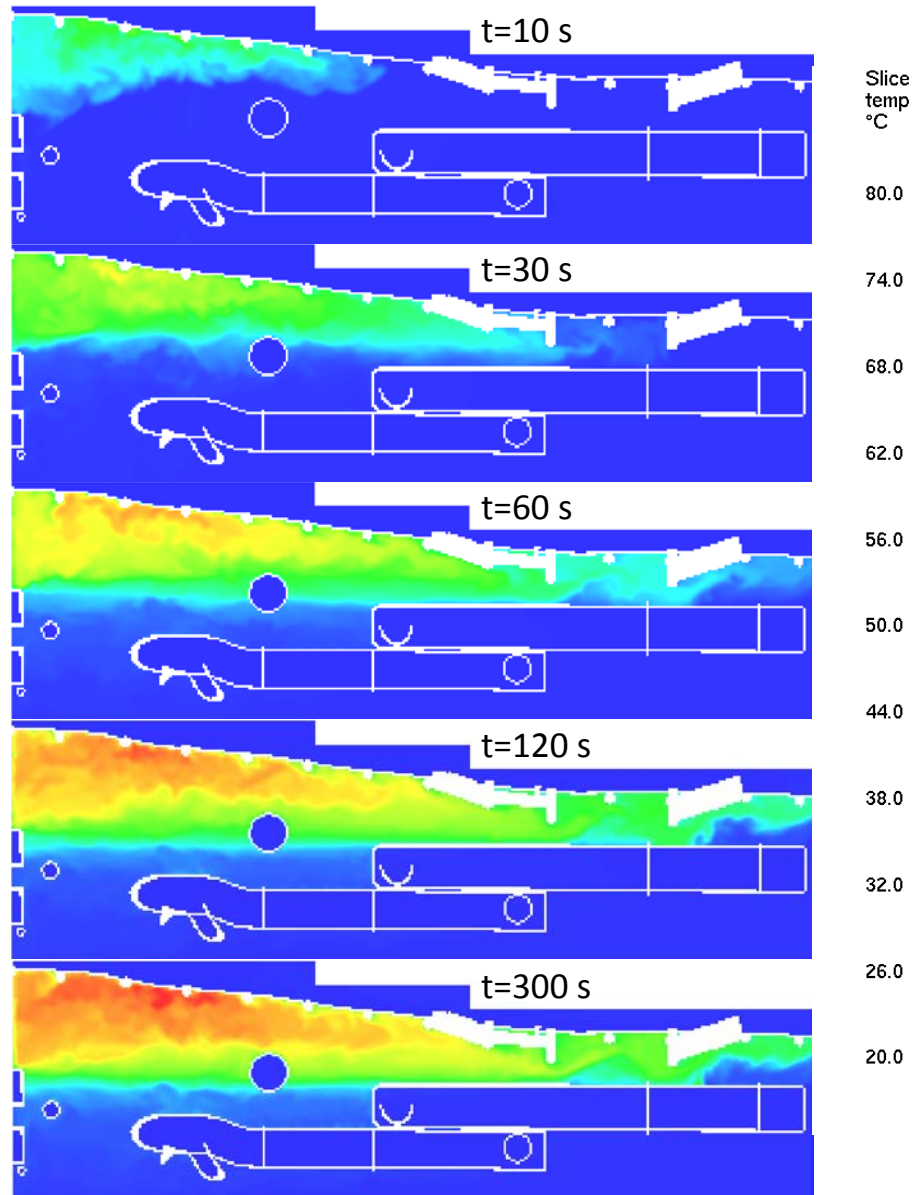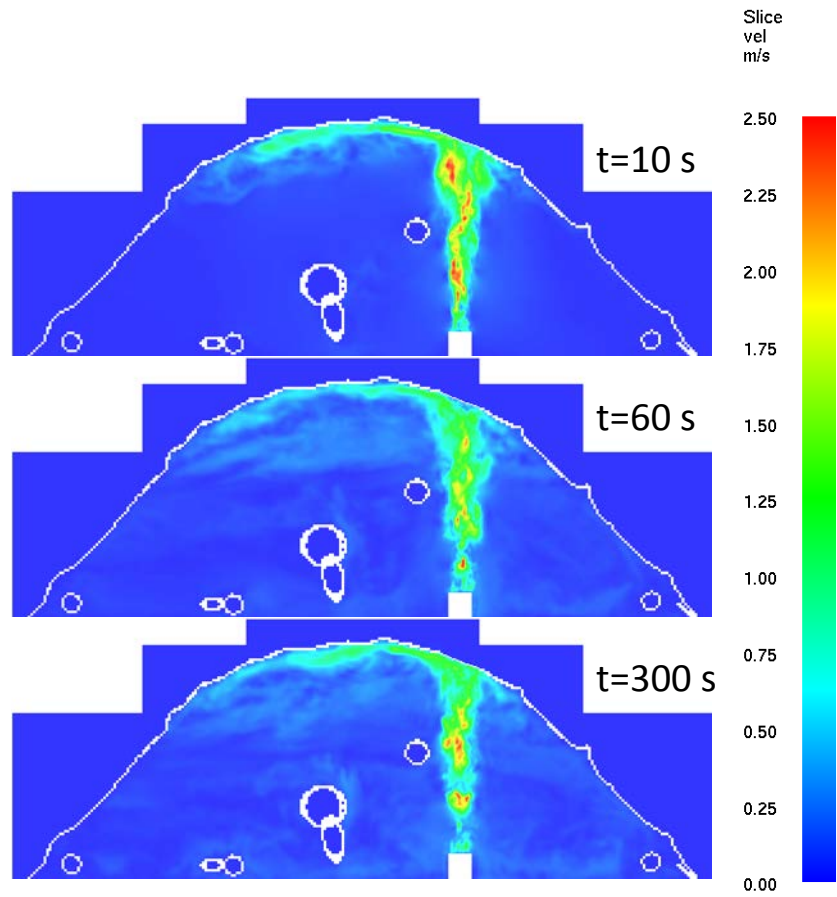
Figure 9. Simulated temperature slice results from normal pressure scenario ($p = 1$ bar) on the *x-z* plane at *y* = 3 m; time was selected at *t* = 10, 30, 60, 120, and 300 s

Figure 10. Simulated temperature slice results from normal pressure scenario (*p* = 1 bar) on the *x-z* plane at *y* = 3.5 m; time was selected at *t* = 10, 30, 60, 120, and 300 s

Figure 11. Simulated velocity slice results from normal pressure scenario (*p* = 1 bar) on the *y-z* plane at *x* = 1.25 m (burner center); time was selected at *t* = 10, 60, and 300 s

Figure 12. Simulated velocity slice results from normal pressure scenario ($p = 1$ bar) on the x-z plane at $y = 2$ m (burner center); time was selected at $t = 10, 60,$ and 300 s
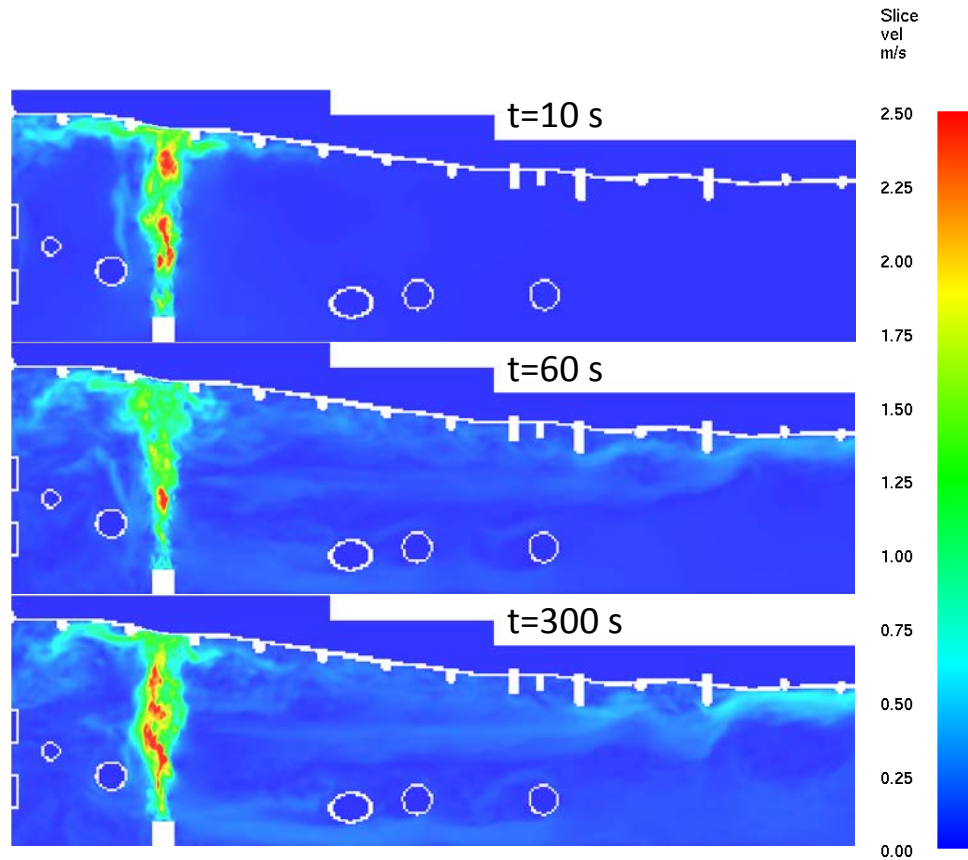
The simulation results were compared with the test results for validation. Figure 13 shows the measured ceiling temperature from representative thermocouples of 18, 20, 22, and 46, along the overhead center. Also shown is the simulated gas temperature at the same location. The simulated temperatures agree well with the measured temperatures. The simulations also successfully predict the time delay within 5 s. The agreement deteriorates at the far end (e.g., TC 46), mostly because of uncertainty in material thermal conductivity. With distance increases, error in conductive heat loss between hot gas and ceiling surface along the ceiling jet path accumulates. It is also noticed that TC 46 is directly below rib 10, where there is more disturbance on the flow.

Figure 14 shows the measured ceiling temperature from representative thermocouples of 42 and 50. These two thermocouples are located at the far edges, as shown in figure 4. Temperatures are close to ambient condition at both sides as ceiling height drops below 0.6 m. The model is able to accurately predict the temperature in these regions.

Figure 15 compares the measured and simulated temperatures from the representative thermocouple tree B. Temperature decreases with the decrease of height. The model is able to predict the temperature at the ceiling and at the bottom. In the middle region, the uncertainty is as high as 15°C.
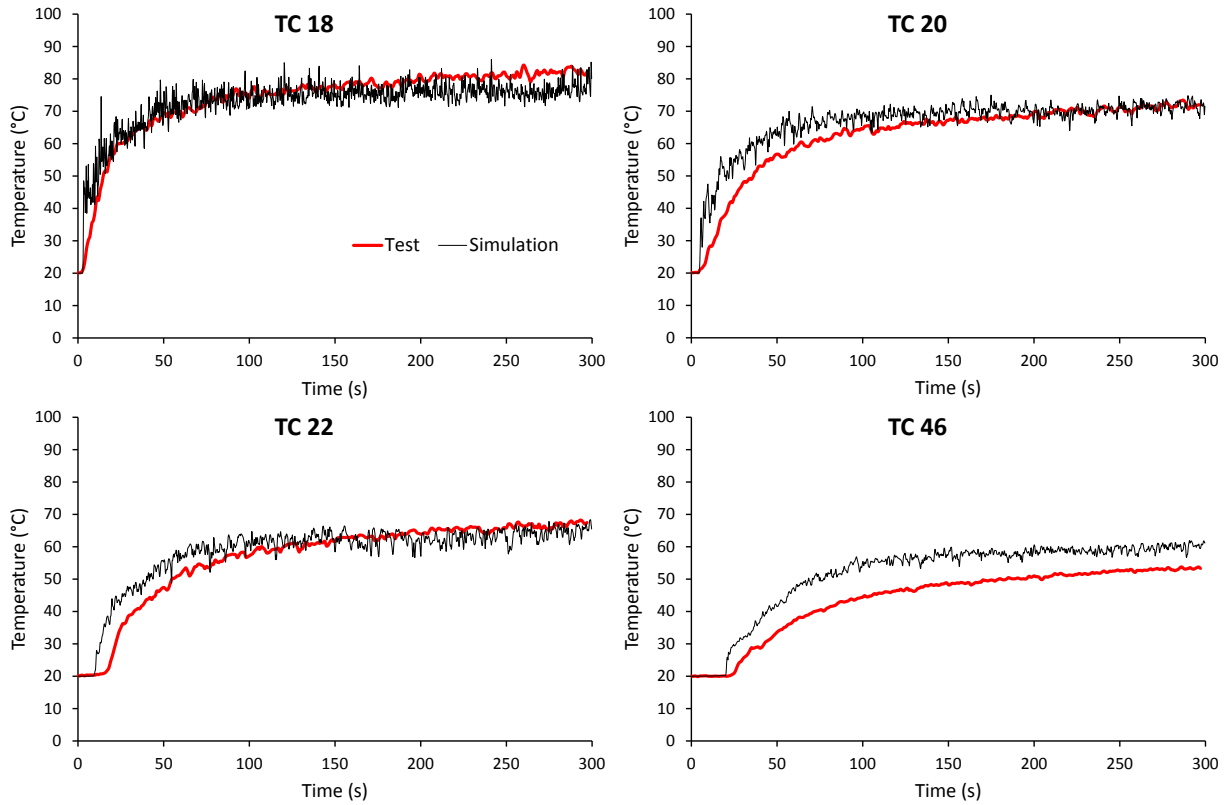
Figure 13. Comparison of the measured and simulated ceiling temperatures from thermocouple 18, 20, 22, and 46, along the overhead center; ambient pressure is at 1 bar
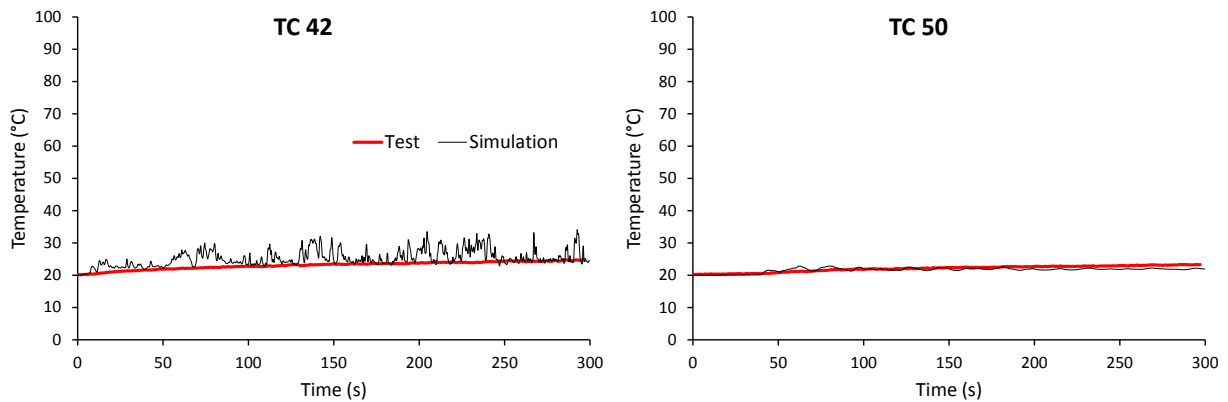
Figure 14. Comparison of the measured and simulated ceiling temperatures from thermocouple 42 and 50 at the overhead area edges; ambient pressure is at 1 bar
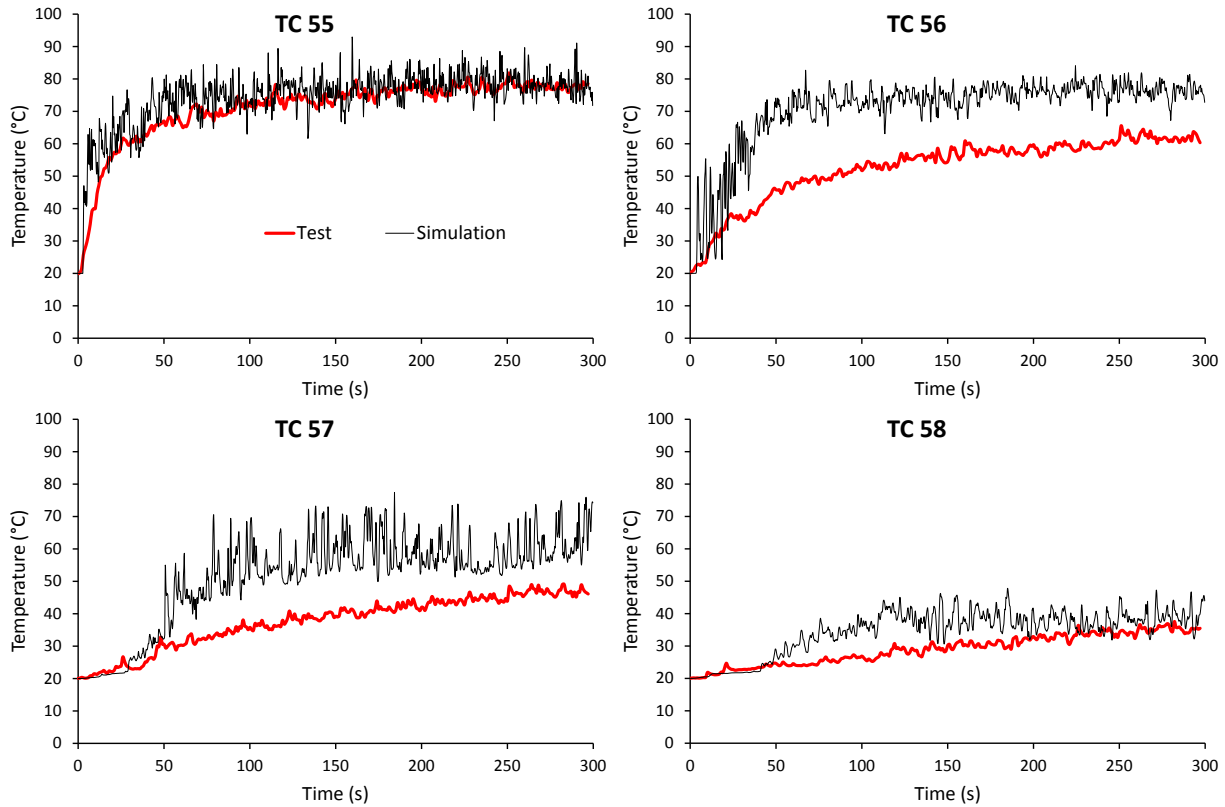
Figure 15. Comparison of the measured and simulated temperatures from thermocouples 55, 56, 57, and 58 at thermocouple tree B; ambient pressure is at 1 bar

The simulated and measured 50 ceiling temperatures were projected on the same *x-y* plane. The resulting contour plots for tests, simulations assuming adiabatic ceiling material, and simulations with real insulation properties, all at steady state, are shown in figures 16–18, respectively. The temperature results are averaged in the last 20 s to suppress data fluctuation. Contour lines are between 30–80°C, with 5 C increments. Because the adiabatic scenario does not account for conductive heat loss, the predicted temperatures are systematically higher than the measured temperatures, especially after $x = 2$ m. The temperature agrees better with the real insulation material properties. The model is also able to predict the temperature transition between $x = 2 - 4$ m.

It is noticed that the hot spot location at the ceiling is slightly different between tests and simulations. In tests, it is directly above the burner center ($x = 1.25$ m, $y = 2$ m) and slightly spans toward the maximum ceiling height location ($y = 2.7$ m). In simulations, the hot spot is centered closer to the maximum ceiling height location. This is presumably because of the difference between thermocouples in tests and gas temperature sensors in simulation. In real tests, thermocouples close to the fire source continuously receive radiation, and its bead temperature is slightly higher than the surrounding gas temperature, whereas in simulations, the gas temperature sensor assumes infinitely small sensor diameter, and its temperature is the same as the surrounding gas temperature [6].

15
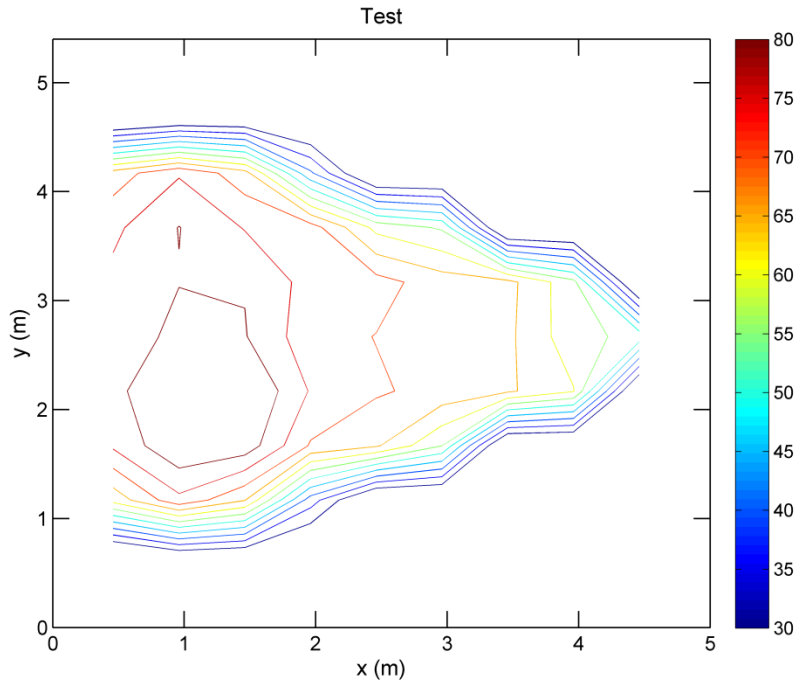
Figure 16. Contour plot of the measured ceiling temperature results at steady state, $t = 300$ s; ambient pressure is at 1 bar
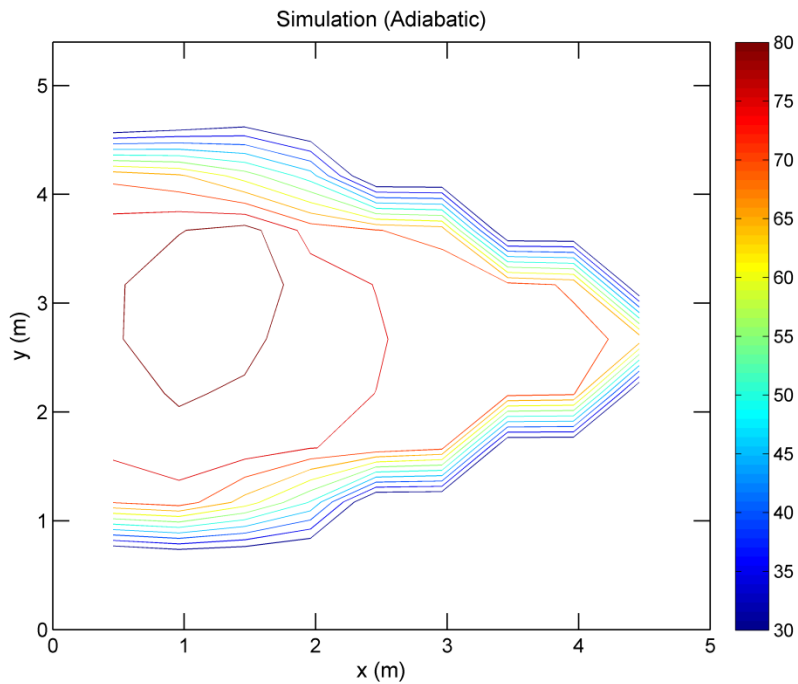
Figure 17. Contour plot of the simulated (adiabatic condition) ceiling temperature results at steady state, $t = 300$ s; ambient pressure is at 1 bar
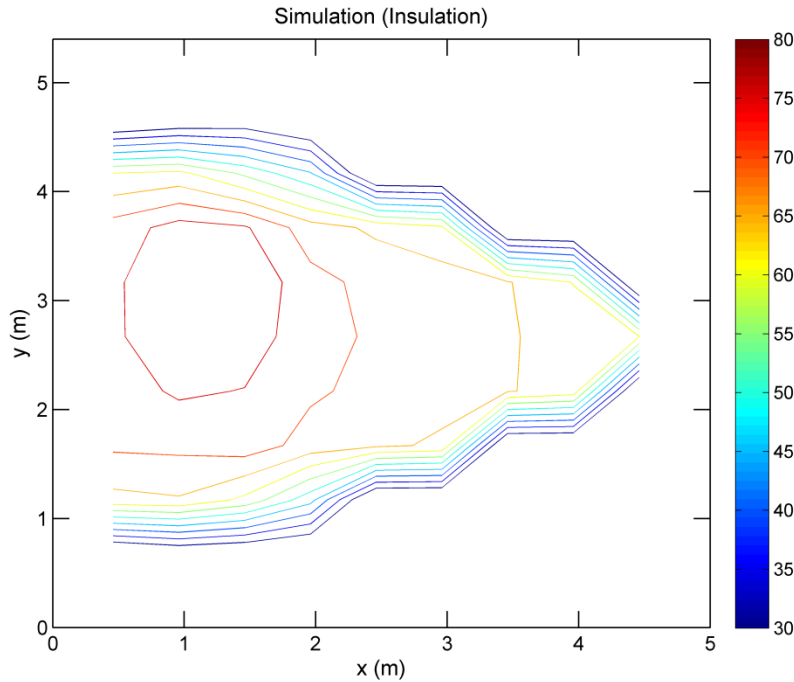
Figure 18. Contour plot of the simulated (insulated condition) ceiling temperature results at steady state, $t = 300$ s; ambient pressure is at 1 bar

3.2 REDUCED PRESSURE RESULTS

The simulated results at reduced pressure ($p = 0.75$ bar) were compared with the simulated results at normal pressure ($p = 1$ bar). A full-scale fire test at reduced pressure is not possible in the test article because of in-flight safety considerations.

Figures 19 and 20 show the simulated temperature slices on the y-z plane at $x = 2.25$ m and on the x-z plane at $y = 3$ m, respectively. Time was chosen at $t = 10, 30, 60, 120,$ and 300 s. These results should be compared with their corresponding simulations at the normal pressure condition shown in figures 7 and 9. The ceiling temperature at the reduced pressure scenario is approximately 5 °C higher than that in the normal pressure.
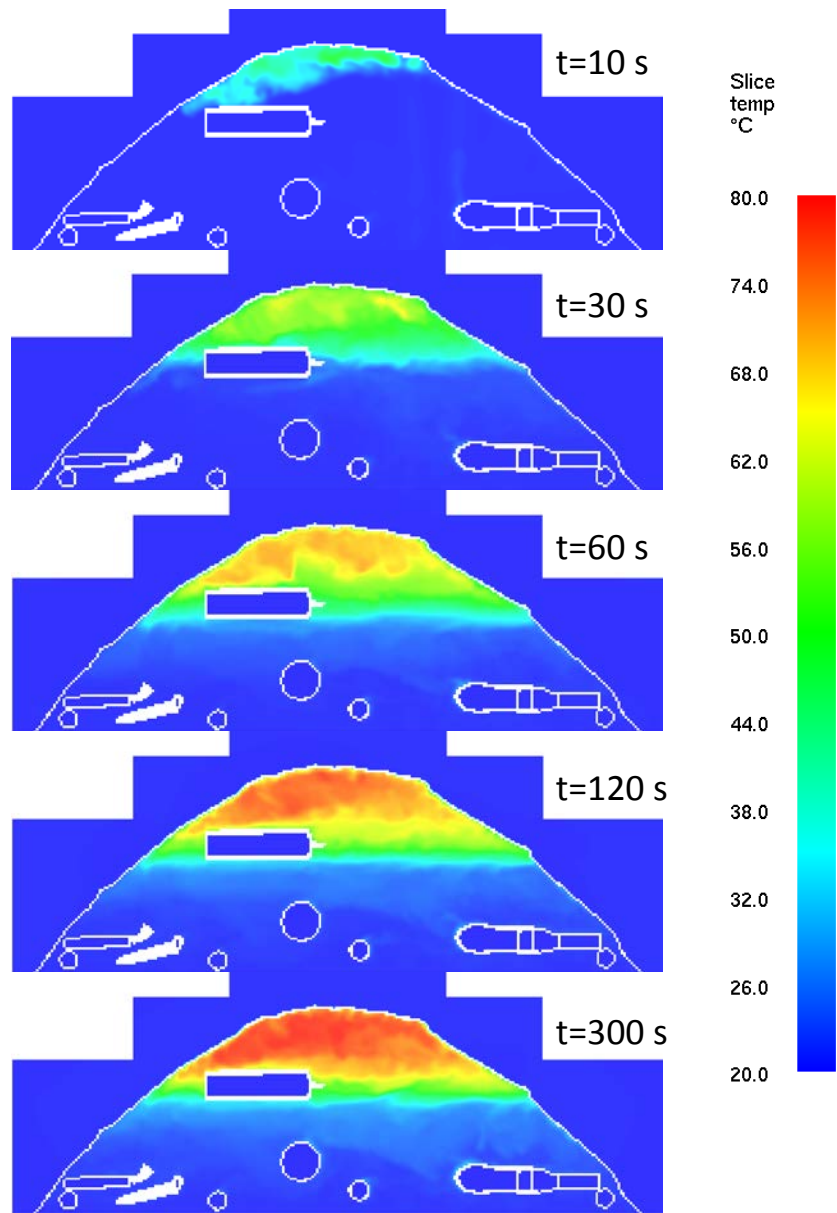
Figure 19. Simulated temperature slice results from reduced pressure scenario (*p* = 0.75 bar) on the *y-z* plane, at *x* = 2.25 m; at times, *t* = 10, 30, 60, 120, and 300 s
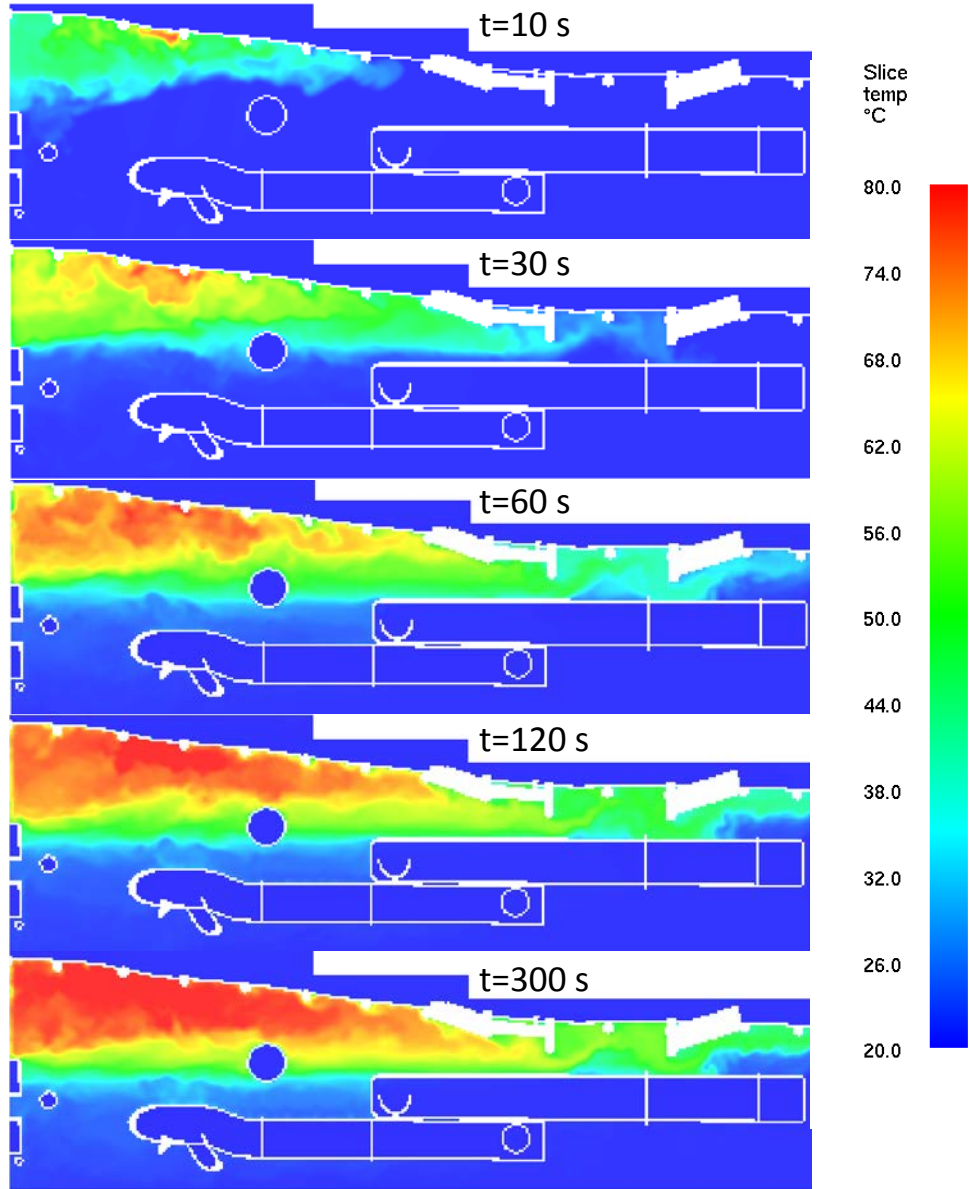
Figure 20. Simulated temperature slice results from reduced pressure scenario ($p = 0.75$ bar) on the *x-z* plane at $y = 3$ m; at times, $t = 10, 30, 60, 120$, and 300 s

This could be explicitly explained by the increased characteristic fire size D^* in Eq. (1). Ambient air density decreases with the decrease of pressure. The characteristic fire size increases accordingly. It can also be speculated that the flame height is proportional to the characteristic fire size [7]. For a point source plume, the dimensionless plume temperature is expressed as [7]:

$$\frac{T - T_\infty}{T_\infty} = C_T \left(\frac{z}{D^*} \right)^{-5/3}$$

(3)

where C_T is the temperature coefficient. For a given flame height, z, T increases with the increase of D^*. Implicitly, it is because the air entrainment strength decreases as buoyancy decreases; the flame envelope expands and the flame height increases to allow more mixing [8]. Entrainment of ambient air into the plume region cools the plume.

The entrainment rate of air into the fire plume is expressed as [7]:

$$\dot{m}_e = \rho_\infty \sqrt{g}\, z^{5/2} C_e \left(\frac{z}{D^*} \right)^{-5/6} \tag{4}$$

where C_e is the entrainment coefficient. Combining Eq. (1) and (4) yields

$$\dot{m}_e = C_e \left(\frac{g z^5 \dot{Q}}{c_p T_\infty} \right)^{1/3} \rho_\infty^{2/3} \tag{5}$$

The entrainment rate falls with the decrease of air density due to decreased pressure. With less entrainment, the cooling effect is decreased, and the plume temperature at the ceiling level increases accordingly.

Detailed comparison of the simulated temperature results for thermocouple locations 18, 20, 22, and 46 are shown in figure 21. These thermocouples are located along the centerline in the y direction. Temperature difference decreases as it approaches the rear side of the overhead area.

Figure 22 shows the contour plot of the simulated temperature results at a pressure of 0.75 bar from the 50 ceiling gas temperature sensor locations. The temperature results were averaged over the last 20 s to suppress data fluctuation.
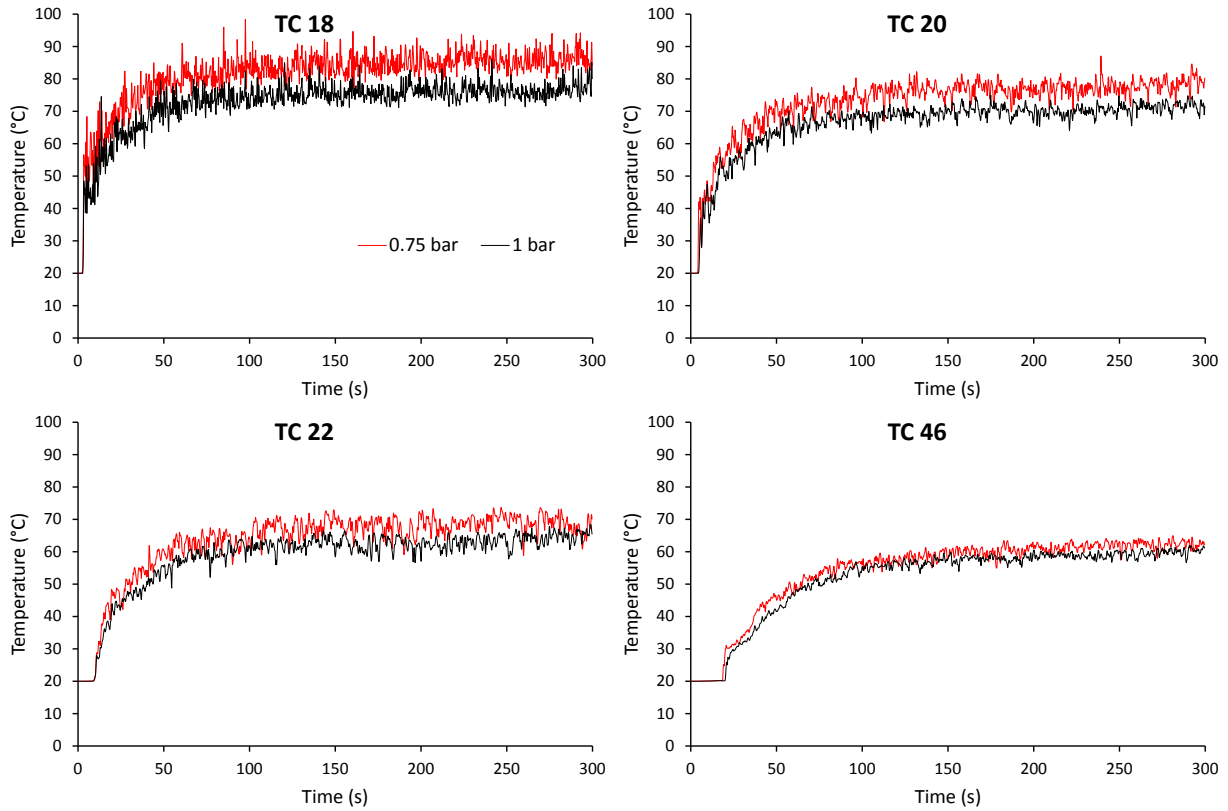
Figure 21. Comparison of the simulated ceiling temperatures at 0.75 and 1 bar; temperatures are from thermocouples 18, 20, 22, and 46 along the overhead center
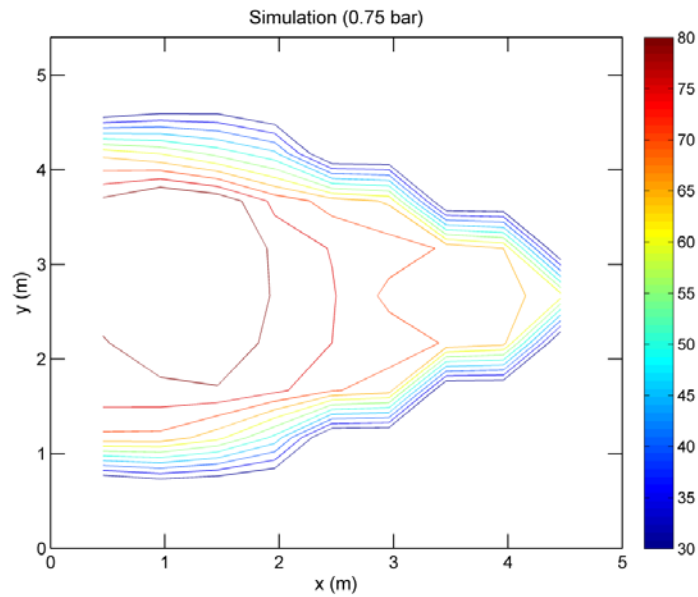

Figure 22. Contour plot of the simulated (insulated condition) ceiling temperature at reduced ambient pressure ($p = 0.75$ bar) results at steady state, $t = 300$ s

3.3 BURNER LOCATION EFFECT

The burner location was shifted along the *x* direction toward the rear (aft) of the overhead area, with its center 1.25 m from the rear of the computation domain. The temperature slice results are in figures 23 and 24. Figure 23 shows the temperatures on the *y-z* plane, at *x* = 2.25 m. Figure 24 shows the temperatures on the *x-z* plane, at *y* = 3, at times, *t* = 10, 30, 60, 120, and 300 s in both figures.
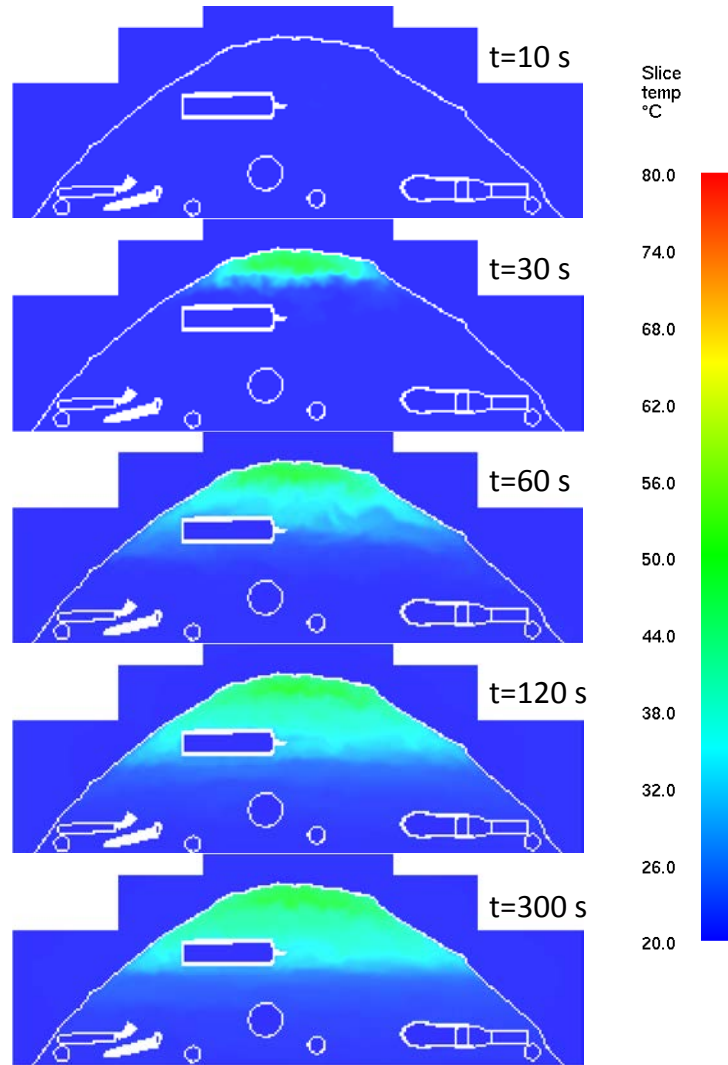
Figure 23. Simulated temperature slice results from normal pressure scenario (*p* = 1 bar) on the *y-z* plane, at *x* = 2.25 m; burner location was shifted toward the rear side of the overhead area, at times, *t* = 10, 30, 60, 120, and 300 s
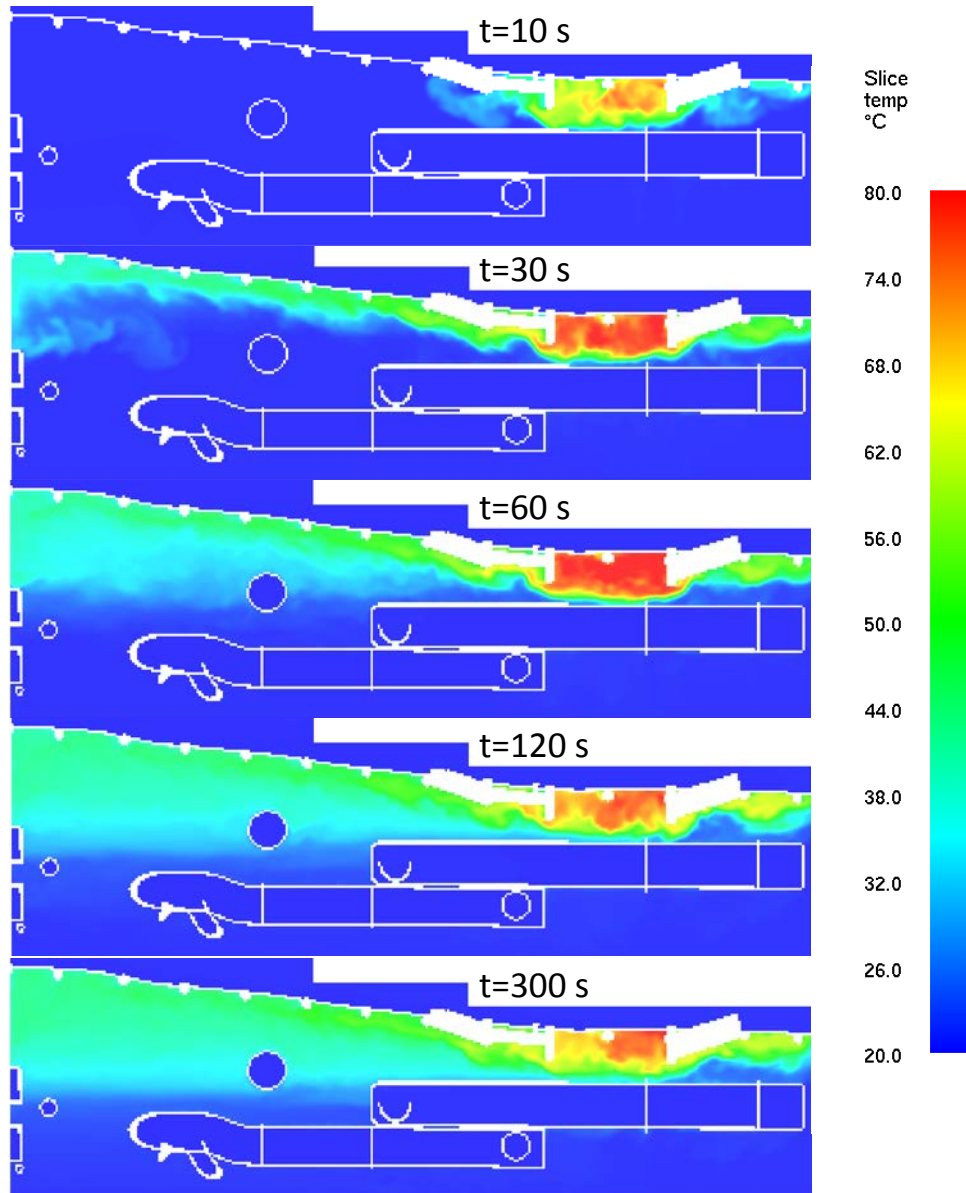
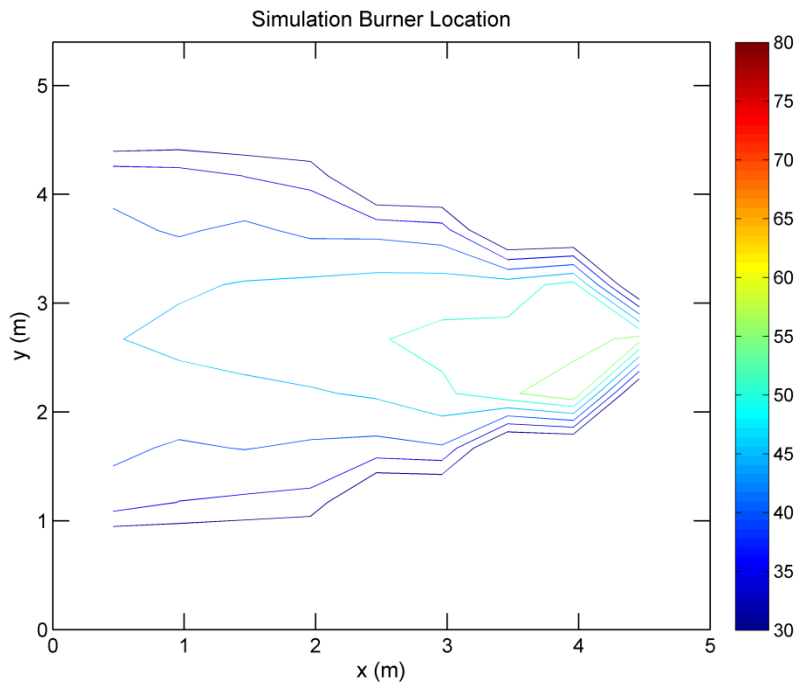**Figure 24. Simulated temperature slice results from normal pressure scenario ($p = 1$ bar) on the *x-z* plane, at $y = 3$ m; the burner location was shifted toward the rear side of the overhead area, and time was selected at $t = 10, 30, 60, 120,$ and 300 s**

The fire source is closer to the open end of the experimental and computational domains, and the hot gases are easier to vent out. Overall, the temperatures are lower than in the corresponding simulations at normal pressure with the burner at its original location.

However, because the burner location is shifted and now the burner is directly under the two large panels (ribs) at the ceiling level (see the hot zones in Fig 24), the hot gases are trapped within the area between these two panels, creating a locally hot zone. Hot gases migrate slowly to the front region of the overhead area because of buoyancy. And the ceiling jet layer accumulates with time. After 60 s, the ceiling jet layer becomes thicker than those two blocking panels, and the convective

23

heat transfer to both the front the region and rear computation domain increases. As a result, the temperature within the region between two blocking panels decreases, as indicated in figure 24 at $t = 120$, and 300 s.

The contour plot of the temperature results at the ceiling level projected on the same x-y plane is shown in figure 25. The gas sensors' locations are kept the same as in the previous simulations. The contour line scale is also kept the same for comparison. Maximum temperature is approximately 55°C with peak temperature closer to the fire source. Because this region is away from the fire source, the temperature gradient along the center line is small. The temperature varies between 45°–55°C.

Figure 25. Contour plot of the simulated (insulated condition) ceiling temperature results at steady state, $t = 300$ s; ambient pressure is at 1 bar, and burner location was shifted toward the rear side of the overhead area

4. CONCLUSIONS AND FUTURE WORKS

An overhead section of a Boeing 747-SP aircraft cabin was used to study heat and smoke movement in a hidden area. Numerical simulations were conducted to analyze the hot gas transport as a result of a simulated hidden fire. The modeled results were compared with full-scale test results and good agreement was observed. Spatially resolved temperature histories were obtained from 50 thermocouples installed horizontally at the ceiling level, and 8 thermocouples installed vertically at 2 thermocouple trees. At the ceiling level, the simulated temperatures agreed with the test results within 5°C for most of the tested region. Further from the fire source, temperature agreement was within 10°C, because of the uncertainty in thermal conductivity of the interior surfaces.

Simulations were also conducted to examine the effect of pressure at cruise altitude on heat transport. The ceiling temperature was found to increase with the decrease of ambient pressure, presumably due to the decreased cooling effect of entrained air and increased flame height at lower pressure.

Also simulated was the effect of fire source location on heat transport. In these simulations the fire source was moved toward the rear (aft) of the overhead area, directly under the two blocking panels at the ceiling level. Hot spots were observed as a result of flow obstruction. As the ceiling jet layer accumulated, convective heat losses to the surrounding area increased and the temperature within the hot spots decreased.

In the future, the transport of heat, smoke, and carbon monoxide/dioxide from burning solid fuels in the cluttered spaces (e.g., cargo compartment, cabin, overhead area) will be studied using the numerical approach. Adequate full-scale test validation will also be performed.

Besides the pressure's effect on fire size, air entrainment, and plume movement, its effect on solid fuel pyrolysis rate and combustion products, especially smoke, have been observed and will be examined in subsequent studies.

The results from the current study, combined with those from the subsequent studies, could be used to guide the placement and certification of smoke detectors, temperature sensors, and CO detectors in transport and cargo aircraft.

5. REFERENCES

1.   AFF. (2014, January). Advisory Circular 120–80. *In-Flight Fires*. Washington DC: U.S. Department of Transportation.

2.   Zhang, Y., Kim, M., Guo, H., Sunderland, P. B., Quintiere, J. G., deRis, J., Stocker, D. P. (2015). Emulation of condensed fuel flames with gases in microgravity. *Combustion and Flame, 162*(10), 3449–3455.

3.   McGrattan, K., Hostikka, S., McDermott, R., Floyd, J., Weinschenk, C., Overholt, K. (2015). *Fire Dynamics Simulator User's Guide*. Gaithersburg, MD: National Institute of Standards and Technology.

4.   Zarzecki, M., Quintiere, J. G., Lyon, R. E., Rossmann, T., Diez, F. J. (2013). The effect of pressure and oxygen concentration on the combustion of PMMA. *Combustion and Flame 160*(8), 1519–1530.

5.   Kim, C. H., El-Leathy, A. M., Xu, F., Faeth, G. M. (2004). Soot surface growth and oxidation in laminar diffusion flames at pressures of 0.1-1.0 atm. *Combustion and Flame, 136*(1–2), 191–207.

6.   Guo, H., Castillo, J. A., Sunderland, P. B. (2013). Digital camera measurements of soot temperature and soot volume fraction in axisymmetric flames. *Applied Optics, 52*(33), 8040–8047.

7.   Quintiere, J. G. (2006). *Fundamentals of fire phenomena*. Hoboken, NJ: John Wiley & Sons, Ltd.

8.   Hu, L., Zhang, X., Zhang, X., Lu, K., Guo, Z. (2017). Flame heights and fraction of stoichiometric air entrained for rectangular turbulent jet fires in a sub-atmospheric pressure. *Proceedings of the Combustion Institute, 36*(2), 2995–3002.